

HESS observations of the Carina nebula and its enigmatic colliding wind binary Eta Carinae

HESS Collaboration, A. Abramowski,¹ F. Acero,² F. Aharonian,^{3,4,5}
A. G. Akhperjanian,^{5,6} G. Anton,⁷ A. Balzer,⁷ A. Barnacka,^{8,9} Y. Becherini,^{10,11}
J. Becker,¹² K. Bernlöhr,^{3,13} E. Birsin,¹³ J. Biteau,¹¹ A. Bochow,³ C. Boisson,¹⁴
J. Bolmont,¹⁵ P. Bordas,¹⁶ J. Brucker,⁷ F. Brun,¹¹ P. Brun,⁹ T. Bulik,¹⁷ I. Büsching,^{12,18}
S. Carrigan,³ S. Casanova,^{3,18} M. Cerruti,¹⁴ P. M. Chadwick,¹⁹ A. Charbonnier,¹⁵
R. C. G. Chaves,^{3,9} A. Cheesebrough,¹⁹ G. Cologna,²⁰ J. Conrad,²¹ M. Dalton,¹³
M. K. Daniel,¹⁹ I. D. Davids,²² B. Degrange,¹¹ C. Deil,³ H. J. Dickinson,²¹
A. Djannati-Ataï,¹⁰ W. Domainko,³ L. O’C. Drury,⁴ G. Dubus,²³ K. Dutson,²⁴ J. Dyks,⁸
M. Dyrda,²⁵ K. Egberts,²⁶ P. Eger,⁷ P. Espigat,¹⁰ L. Fallon,⁴ S. Fegan,¹¹ F. Feinstein,²
M. V. Fernandes,¹ A. Fiasson,²⁷ G. Fontaine,¹¹ A. Förster,³ M. Füßling,¹³
Y. A. Gallant,² T. Garrigoux,¹⁵ H. Gast,³ L. Gérard,¹⁰ B. Giebels,¹¹ J. F. Glicenstein,⁹
B. Glück,⁷ D. Göring,⁷ M.-H. Grondin,^{3,20} S. Häffner,⁷ J. D. Hague,³ J. Hahn,³
D. Hampf,¹ J. Harris,¹⁹ M. Hauser,²⁰ S. Heinz,⁷ G. Heinzelmann,¹ G. Henri,²³
G. Hermann,³ A. Hillert,³ J. A. Hinton,²⁴ W. Hofmann,³ P. Hofverberg,³ M. Holler,⁷
D. Horns,¹ A. Jacholkowska,¹⁵ C. Jahn,⁷ M. Jamrozny,²⁸ I. Jung,⁷ M. A. Kastendieck,¹
K. Katarzyński,²⁹ U. Katz,⁷ S. Kaufmann,²⁰ B. Khélifi,¹¹ D. Klochkov,¹⁶ W. Kluźniak,⁸
T. Kneiske,¹ Nu. Komin,²⁷ K. Kosack,⁹ R. Kossakowski,²⁷ F. Krayzel,²⁷ H. Laffon,¹¹
G. Lamanna,²⁷ J.-P. Lenain,²⁰ D. Lennarz,³ T. Lohse,¹³ A. Lopatin,⁷ C.-C. Lu,³
V. Marandon,³ A. Marcowith,² J. Masbou,²⁷ G. Maurin,²⁷ N. Maxted,³⁰ M. Mayer,⁷
T. J. L. McComb,¹⁹ M. C. Medina,⁹ J. Méhault,² R. Moderski,⁸ M. Mohamed,²⁰
E. Moulin,⁹ C. L. Naumann,¹⁵ M. Naumann-Godo,⁹ M. de Naurois,¹¹ D. Nedbal,³¹
D. Nekrassov,³ N. Nguyen,¹ B. Nicholas,³⁰ J. Niemiec,²⁵ S. J. Nolan,¹⁹ S. Ohm,^{3,24,32★}
E. de Oña Wilhelmi,³ B. Opitz,¹ M. Ostrowski,²⁸ I. Oya,¹³ M. Panter,³
M. Paz Arribas,¹³ N. W. Pekeur,¹⁸ G. Pelletier,²³ J. Perez,²⁶ P.-O. Petrucci,²³
B. Peyaud,⁹ S. Pita,¹⁰ G. Pühlhofer,¹⁶ M. Punch,¹⁰ A. Quirrenbach,²⁰ M. Raue,¹
A. Reimer,²⁶ O. Reimer,²⁶ M. Renaud,² R. de los Reyes,³ F. Rieger,^{3,33} J. Ripken,²¹
L. Rob,³¹ S. Rosier-Lees,²⁷ G. Rowell,³⁰ B. Rudak,⁸ C. B. Rulten,¹⁹ V. Sahakian,^{5,6}
D. A. Sanchez,³ A. Santangelo,¹⁶ R. Schlickeiser,¹² A. Schulz,⁷ U. Schwanke,¹³
S. Schwarzburg,¹⁶ S. Schwemmer,²⁰ F. Sheidaei,^{10,18} J. L. Skilton,³ H. Sol,¹⁴
G. Spengler,¹³ Ł. Stawarz,²⁸ R. Steenkamp,²² C. Stegmann,⁷ F. Stinzing,⁷ K. Stycz,⁷
I. Sushch,¹³ A. Szostek,²⁸ J.-P. Tavernet,¹⁵ R. Terrier,¹⁰ M. Tluczykont,¹ K. Valerius,⁷
C. van Eldik,^{3,7} G. Vasileiadis,² C. Venter,¹⁸ A. Viana,⁹ P. Vincent,¹⁵ H. J. Völk,³

*E-mail: stefan.ohm@le.ac.uk

F. Volpe,³ S. Vorobiov,² M. Vorster,¹⁸ S. J. Wagner,²⁰ M. Ward,¹⁹ R. White,²⁴
 A. Wiercholska,²⁸ M. Zacharias,¹² A. Zajczyk,^{2,8} A. A. Zdziarski,⁸ A. Zech,¹⁴
 H.-S. Zechlin¹ and T. Montmerle³⁴

¹Universität Hamburg, Institut für Experimentalphysik, Luruper Chaussee 149, D 22761 Hamburg, Germany

²Laboratoire Univers et Particules de Montpellier, Université Montpellier 2, CNRS/IN2P3, CC 72, Place Eugène Bataillon, F-34095 Montpellier Cedex 5, France

³Max-Planck-Institut für Kernphysik, PO Box 103980, D 69029 Heidelberg, Germany

⁴Dublin Institute for Advanced Studies, 31 Fitzwilliam Place, Dublin 2, Ireland

⁵National Academy of Sciences of the Republic of Armenia, 0019 Yerevan, Armenia

⁶Yerevan Physics Institute, 2 Alikhanian Brothers St., 375036 Yerevan, Armenia

⁷Universität Erlangen-Nürnberg, Physikalisches Institut, Erwin-Rommel-Str. 1, D 91058 Erlangen, Germany

⁸Nicolaus Copernicus Astronomical Center, ul. Bartycka 18, 00-716 Warsaw, Poland

⁹CEA Saclay, DSM/IRFU, F-91191 Gif-Sur-Yvette Cedex, France

¹⁰APC, AstroParticule et Cosmologie, Université Paris Diderot, CNRS/IN2P3, CEA/Ifju, Observatoire de Paris, Sorbonne Paris Cité, 10, rue Alice Domon et Léonie Duquet, 75205 Paris Cedex 13, France

¹¹Laboratoire Leprince-Ringuet, Ecole Polytechnique, CNRS/IN2P3, F-91128 Palaiseau, France

¹²Institut für Theoretische Physik, Lehrstuhl IV: Weltraum und Astrophysik, Ruhr-Universität Bochum, D 44780 Bochum, Germany

¹³Institut für Physik, Humboldt-Universität zu Berlin, Newtonstr. 15, D 12489 Berlin, Germany

¹⁴LUTH, Observatoire de Paris, CNRS, Université Paris Diderot, 5 Place Jules Janssen, 92190 Meudon, France

¹⁵LPNHE, Université Pierre et Marie Curie Paris 6, Université Denis Diderot Paris 7, CNRS/IN2P3, 4 Place Jussieu, F-75252 Paris Cedex 5, France

¹⁶Institut für Astronomie und Astrophysik, Universität Tübingen, Sand 1, D 72076 Tübingen, Germany

¹⁷Astronomical Observatory, The University of Warsaw, Al. Ujazdowskie 4, 00-478 Warsaw, Poland

¹⁸Unit for Space Physics, North-West University, Potchefstroom 2520, South Africa

¹⁹Department of Physics, University of Durham, South Road, Durham DH1 3LE

²⁰Landessternwarte, Universität Heidelberg, Königstuhl, D 69117 Heidelberg, Germany

²¹Oskar Klein Centre, Department of Physics, Stockholm University, Albanova University Center, SE-10691 Stockholm, Sweden

²²Department of Physics, University of Namibia, Private Bag 13301, Windhoek, Namibia

²³Laboratoire d'Astrophysique de Grenoble, INSU/CNRS, Université Joseph Fourier, BP 53, F-38041 Grenoble Cedex 9, France

²⁴Department of Physics and Astronomy, The University of Leicester, University Road, Leicester LE1 7RH

²⁵Instytut Fizyki Jądrowej PAN, ul. Radzikowskiego 152, 31-342 Kraków, Poland

²⁶Institut für Astro- und Teilchenphysik, Leopold-Franzens-Universität Innsbruck, A-6020 Innsbruck, Austria

²⁷Laboratoire d'Annecy-le-Vieux de Physique des Particules, Université de Savoie, CNRS/IN2P3, F-74941 Annecy-le-Vieux, France

²⁸Obserwatorium Astronomiczne, Uniwersytet Jagielloński, ul. Orla 171, 30-244 Kraków, Poland

²⁹Toruń Centre for Astronomy, Nicolaus Copernicus University, ul. Gagarina 11, 87-100 Toruń, Poland

³⁰School of Chemistry & Physics, University of Adelaide, Adelaide 5005, Australia

³¹Charles University, Faculty of Mathematics and Physics, Institute of Particle and Nuclear Physics, V Holešovičkách 2, 180 00 Prague 8, Czech Republic

³²School of Physics & Astronomy, University of Leeds, Leeds LS2 9JT

³³European Associated Laboratory for Gamma-Ray Astronomy, jointly supported by CNRS and MPG

³⁴Institut d'Astrophysique de Paris, 98bis, Bd Arago, 75014 Paris, France

Accepted 2012 April 24. Received 2012 April 24; in original form 2012 March 27

ABSTRACT

The massive binary system Eta Carinae and the surrounding H II complex, the Carina nebula, are potential particle acceleration sites from which very high energy (VHE; $E \geq 100$ GeV) γ -ray emission could be expected. This paper presents data collected during VHE γ -ray observations with the HESS telescope array from 2004 to 2010, which cover a full orbit of Eta Carinae. In the 33.1-h data set no hint of significant γ -ray emission from Eta Carinae has been found and an upper limit on the γ -ray flux of 7.7×10^{-13} ph cm⁻² s⁻¹ (99 per cent confidence level) is derived above the energy threshold of 470 GeV. Together with the detection of high energy (HE; $0.1 \leq E \leq 100$ GeV) γ -ray emission by the *Fermi* Large Area Telescope up to 100 GeV, and assuming a continuation of the average HE spectral index into the VHE domain, these results imply a cut-off in the γ -ray spectrum between the HE and VHE γ -ray range. This could be caused either by a cut-off in the accelerated particle distribution or by severe γ - γ absorption losses in the wind collision region. Furthermore, the search for extended γ -ray emission from the Carina nebula resulted in an upper limit on the γ -ray flux of 4.2×10^{-12} ph cm⁻² s⁻¹ (99 per cent confidence level). The derived upper limit of ~ 23 on the cosmic ray enhancement factor is compared with results found for the old-age mixed-morphology supernova remnant W28.

Key words: acceleration of particles – radiation mechanisms: non-thermal – ISM: individual objects: Carina nebula – ISM: individual objects: Eta Carinae – open clusters and associations: general – X-rays: binaries.

1 INTRODUCTION

The Carina nebula is one of the largest and most active H II regions in our Galaxy and a place of ongoing star formation. It is located at a distance of ~ 2.3 kpc and harbours eight open stellar clusters with more than 66 O-type stars, three Wolf–Rayet stars and the luminous blue variable (LBV) Eta Carinae (Feinstein 1995; Smith 2006; Smith & Brooks 2008). The existence of a $\sim 10^6$ -yr-old neutron star indicates past supernova (SN) activity in the Carina complex (Hamaguchi et al. 2009; Pires et al. 2009). The age estimates of the member clusters Trumpler 14, 15 and 16 vary significantly, with an age spread of ~ 2 Myr to ~ 8 Myr, indicating several past episodes of star formation in the northern region; more recent star formation is going on in the southern part of the nebula (see Preibisch et al. 2011a, and references therein). Extended X-ray emission has been reported by e.g. Hamaguchi et al. (2007) based on observations with *Suzaku*, supplemented by *XMM–Newton* (Ezoe et al. 2008) and *Chandra* (Townsend et al. 2011) observations. These authors found a very low nitrogen-to-oxygen ratio, which, in addition to the presence of a neutron star, suggests that the diffuse plasma originates in one or several unrecognized supernova remnants (SNRs), in particular in the area surrounding Eta Carinae. The emission may also be attributed to stellar winds from massive stars. In their ~ 1.4 deg $^{-2}$ survey of the diffuse X-ray emission, Townsend et al. (2011) also found evidence for a significant contribution due to charge exchange. This mechanism would originate in a contact layer between the hot plasma and the cold molecular clouds (MCs).

Eta Carinae, a member star of Trumpler 16 (Tr 16), is one of the most peculiar objects in our Galaxy, whose environment shows traces of massive eruptions that occurred in past epochs. A giant outburst in the 1840s (known as the Great Eruption) and a smaller outburst in the 1890s produced the Homunculus and little Homunculus Nebulae, respectively (see e.g. Ishibashi et al. 2003). The material expelled from the central star in the Great Eruption has a combined mass of $\sim 12 M_{\odot}$ and moves outwards at an average speed of ~ 650 km s $^{-1}$, implying a kinetic energy of roughly $(4\text{--}10) \times 10^{49}$ erg (Smith et al. 2003). Smith (2008) found material that is moving ahead of the expanding Homunculus Nebula at speeds of 3500–6000 km s $^{-1}$, which doubles the estimate of the kinetic energy of the giant outburst. For a long time it was believed that the central object, Eta Carinae, is a single, hypergiant LBV star – one of only very few found in the Galaxy (see e.g. Clark, Larionov & Arkharov 2005). However, observations now suggest Eta Carinae to be composed of a massive LBV star and an O- or B-type companion star (Hillier et al. 2001; Pittard & Corcoran 2002). The present-day period of the binary has been estimated to $P_{\text{orb}} = 2022.7 \pm 1.2$ d (Damineli et al. 2008), its eccentricity to be $e \sim 0.9$ (Nielsen et al. 2007) and the semimajor axis to be $a = 16.64$ au (Hillier et al. 2001). The LBV star has a very high mass loss rate of $\dot{M}_1 \geq 5 \times 10^{-4} M_{\odot} \text{ yr}^{-1}$ (Hillier et al. 2001; Parkin et al. 2009) and a terminal wind velocity of $v_1 \sim (500\text{--}700)$ km s $^{-1}$; the companion star has a thin, fast wind ($\dot{M}_2 \sim 1.0 \times 10^{-5} M_{\odot} \text{ yr}^{-1}$ and $v_2 \sim 3000$ km s $^{-1}$; Pittard & Corcoran 2002). The total kinetic energy in stellar winds is of the order of a few $\times 10^{37}$ erg s $^{-1}$ for the LBV and the OB star together.

When stellar winds of such stars collide, they form a stellar wind shock, where particles can be accelerated to non-thermal energies (e.g. Eichler & Usov 1993; Reimer, Pohl & Reimer 2006). There is strong evidence for the existence of non-thermal particles in Eta Carinae based on X-ray measurements performed with the instruments aboard the *INTEGRAL* (Leyder, Walter & Rauw 2008, 2010) and *Suzaku* satellites (Sekiguchi et al. 2009). In the high-energy (HE; $100 \text{ MeV} \leq E \leq 100 \text{ GeV}$) domain, the *AGILE* (Tavani et al. 2009) and *Fermi* Large Area Telescope (LAT; Abdo et al. 2009, 2010a,b; Nolan et al. 2012) collaborations have reported on the detection of a source coincident with Eta Carinae (henceforth 2FGL J1045.0–5941). Recently Farnier, Walter & Leyder (2011) confirmed with the *Fermi*-LAT data the position of the HE γ -ray source and extracted an energy spectrum which features a low-energy and a high-energy component. The HE component extends up to ~ 100 GeV, close to the energy threshold of the HESS telescope array. The *AGILE* collaboration reported on a two-day γ -ray flare from the direction of Eta Carinae which occurred in 2008 October. Although this increased γ -ray flux could not be confirmed by Farnier et al. (2011), Walter & Farnier (2011) found that the HE component flux shows a drop in the yearly light curve. Both these findings point to a possible origin of the HE γ -ray emission in the colliding wind region of Eta Carinae.

TeV J2032+4130 (Aharonian et al. 2002), HESS J1023–575 (Aharonian et al. 2007a) and the extended very high energy (VHE) γ -ray emission seen from the vicinity of Westerlund 1 (Abramowski et al. 2012) seem to indicate that VHE γ -ray emission can be linked to massive stars in our Galaxy and motivates an investigation of Eta Carinae and the Carina region as a whole as potential VHE γ -ray emitters. A further motivation comes from the detection of γ -ray emission from binary star systems such as LS 5039 (Aharonian et al. 2006c), PSR B1259–63 (Aharonian et al. 2005), LS I+61 303 (Albert et al. 2006) and the probable TeV binary HESS J0632+057 (Aharonian et al. 2007b; Bongiorno et al. 2011). Note that, unlike Eta Carinae these objects have a compact object (a neutron star or black hole) as stellar companion. Furthermore, the recent detection of HE γ -ray emission up to 100 GeV from the direction of Eta Carinae might hint at particle acceleration up to the VHE γ -ray regime in which HESS is operating.

2 HESS OBSERVATIONS

2.1 HESS experiment

HESS is an array of four VHE γ -ray imaging atmospheric Cherenkov telescopes (IACTs) located in the Khomas Highland of Namibia. Each of these telescopes is equipped with a tessellated spherical mirror of 107 m 2 area and a camera comprising 960 photomultiplier (PMT) tubes, covering a large field of view (FoV) of 5 $^{\circ}$ diameter. The system works in a coincidence mode, requiring at least two of the four telescopes to detect the same extended air shower. This stereoscopic approach results in an angular resolution of ~ 6 arcmin per event, a good energy resolution (15 per cent on average) and an efficient rejection of the hadronic background (selection cuts retain less than 0.01 per cent of the cosmic

Table 1. Properties of the data sets used to calculate the flux upper limits and the light curve shown in Figs 2 and 3, respectively. The time range of the HESS observations and the total live time corresponding to the individual data sets along with the covered orbital phase are summarized.

Data set	Date	MJD	Phase	Live time (h)
1	24.03.04	53088	0.12	1.4
2	11.02.05	53412	0.29	0.9
3	22.05.06–24.05.06	53877–53879	0.52	5.0
4	01.02.09–14.04.09	54863–54935	1.01–1.04	1.8
5	15.01.10–22.03.10	55211–55277	1.18–1.21	18.4
6	06.12.10–18.12.10	55536–55548	1.34–1.35	5.6
All	24.03.04–18.12.10	53088–55548	0.12–1.35	33.1

rays (CRs); Benbow 2005). HESS has a point-source sensitivity of $\sim 2 \times 10^{-13}$ ph cm $^{-2}$ s $^{-1}$ within 25 h of observations (Aharonian et al. 2006a). This flux level corresponds to a 1 per cent integral flux of the Crab nebula for energies $E > 0.2$ TeV, and detection threshold of 5σ (Li & Ma 1983). The more advanced data analysis method that is used in this work is discussed later, and achieves a significantly better point-source sensitivity (Ohm, van Eldik & Egberts 2009).

2.2 Data set

Observations of the (Sagittarius-) Carina arm tangent have been carried out as part of the HESS Galactic plane survey (Aharonian et al. 2006b, 2008a). Additionally, observations pointing in the direction of Eta Carinae have been performed in the so-called *wobble-mode*, where the telescopes were alternately pointed offset in RA and Dec. from Eta Carinae (Aharonian et al. 2006a). The Carina region and its surroundings were observed with the HESS array for a total of 62.4 h between 2004 and 2010. After standard data quality selection, where data taken under unstable weather conditions or with malfunctioning hardware have been excluded, the total exposure time after dead time correction of 3 to 4 telescope data is 33.1 h (Aharonian et al. 2006a). Due to Eta Carinae’s very southern position on the sky, observations have been carried out at moderate zenith angles of 36° – 54° , with a mean value of 39° . The average pointing offset from Eta Carinae was 0.8° .

2.3 Data analysis

The available data have been analysed with the HESS Standard Analysis for shower reconstruction (Aharonian et al. 2006a) and the Hillas-based Boosted Decision Trees (BDT) method for an efficient suppression of the hadronic background component.¹ This machine-learning algorithm returns a continuous variable (called ζ) that was used to select γ -ray-like events. Compared to the HESS Standard Analysis, a cut on this parameter results in an improvement in terms of sensitivity of ~ 20 per cent for spectral and morphological analysis. For the generation of sky images, the spectral analysis and the production of light curves, the $\zeta_{\text{std-cuts}}$ with a 60 photoelectron (p.e.) cut on the image intensity has been applied (see Ohm et al. 2009). The usage of this set of cuts leads to an energy threshold of 470 GeV for these observations. The 68 per cent containment radius of the HESS point spread function (PSF) for the analysis presented here is 6.7 arcmin.

¹ The HESS Analysis Package (HAP) version 11-02-pl07 has been used to analyse the data set presented in this work.

In order to search for a γ -ray signal from Eta Carinae and the Carina nebula, two different background estimation techniques have been employed, i.e. the *ring* background and the *reflected* background model (Berge, Funk & Hinton 2007). The former has been applied to produce two-dimensional sky images, whereas the latter method has been used to derive spectral information and light curves. Table 1 summarizes the properties of the different data sets used in this work and the orbital phases of Eta Carinae which are covered by HESS observations. Note that throughout the paper the orbital phase is defined as phase angle with reference zero-time MJD 52822.492 corresponding to the periastron passage, and a period of 2022.7 d (Damineli et al. 2008).

Observations have been carried out over a time span of six years, during which the reflectivity of the HESS mirrors varied and the gains of the PMTs changed. The energy scale of the instrument is calibrated by looking at the response to single muons (Aharonian et al. 2006a).

Two different circular regions have been selected a priori and have been searched for a signal in the HESS data. Both of them are shown in Fig. 1 and are centred on the Eta Carinae position at RA $10^{\text{h}}45^{\text{m}}03^{\text{s}}.6$ and Dec. $-59^\circ41'04''.3$ (J2000). Given the size

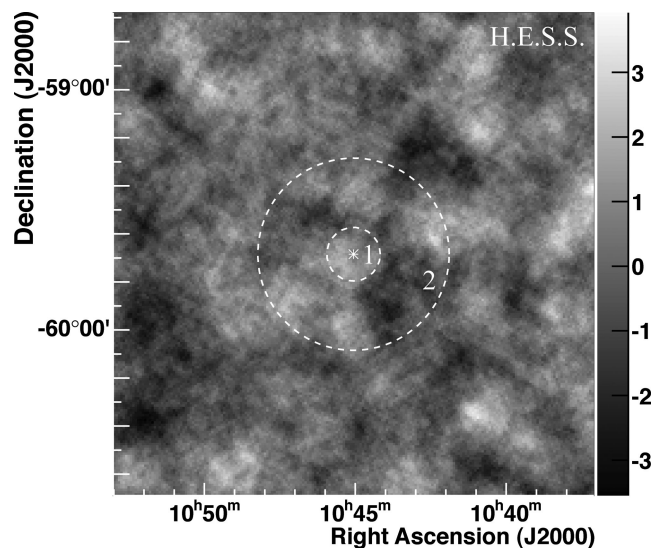


Figure 1. HESS significance map of the $2^\circ \times 2^\circ$ region around Eta Carinae, generated with an oversampling radius of 6.7 arcmin, corresponding to the PSF of this analysis, and calculated according to Li & Ma (1983). Circles denote the integration radii (*Region 1* and *Region 2*) which were used to extract the statistics as given in the text and the upper limits depicted in Fig. 2.

of the Eta Carinae system of $\mathcal{O}(1 \text{ arcmin})$, any VHE γ -ray signal would appear point-like to HESS (*Region 1*, 0.112 radius). The Carina nebula, on the other hand, is a large and complex reflection nebula which shows extended emission seen in mid-infrared (mid-IR), optical and X-ray wavelengths on scales of $\sim 1^\circ \times 2.5$. The second circular region (*Region 2*, 0.4 radius) has a physical scale of 16 pc at 2.3 kpc distance and has been chosen such that the bulk of the diffuse X-ray emission (Townsley et al. 2011) and potential particle acceleration sites such as the massive young stellar clusters Tr 14, and Tr 16 are encompassed. *Region 2* also encloses most of the $H\alpha$ (Smith, Bally & Walborn 2010) and $8 \mu\text{m}$ emission which traces gaseous and dusty material.

All results presented in the following have been successfully checked for consistency with an analysis chain that is based on a different shower reconstruction method and γ -ray selection criteria (de Naurois & Rolland 2009), and on a different calibration. During data taking, increased and variable single-telescope rates and, after quality selection, an increased but stable system trigger rate have been observed. This can be ascribed to the very high night-sky-background (NSB) level caused by the strong ultraviolet emission from the Carina nebula. This NSB level is higher than in any other HESS FoV from which results have been reported so far. Systematic tests have been performed and show that predominantly events which result in shower images with intensities below 60 p.e. are affected. However, the high NSB level does not affect the results presented here, since only events with image sizes greater than 60 p.e. are used. Moreover, the main analysis and the cross-check analysis – which models the NSB for shower reconstruction (de Naurois & Rolland 2009) – give consistent results.

2.4 VHE γ -ray results

Fig. 1 shows the VHE γ -ray significance map of the $2^\circ \times 2^\circ$ region centred on the optical position of Eta Carinae, and calculated according to Li & Ma (1983). The map has been obtained with the *ring* background method and for an integration angle of 6.7 arcmin . No evidence for significant VHE γ -ray emission is found from *Region 1* or from *Region 2*. Assuming a point-like source at the position of Eta Carinae (*Region 1*), a total of 40 ± 26 excess events with a significance of 1.6σ are found. Within *Region 2*, 197 ± 101 excess events with a significance of 2.0σ are detected.

Upper limits (ULs) for the VHE γ -ray emission from Eta Carinae and the extended region of 0.4 radius which covers the inner parts of the Carina nebula have been produced. Fig. 2 shows the 99 per cent ULs (following Feldman & Cousins 1998) on the VHE γ -ray flux from Eta Carinae and the Carina region, assuming an underlying power-law distribution $dN/dE = \Phi_0(E/1 \text{ TeV})^{-\Gamma}$ with photon index $\Gamma = 2.0$. Adjusting the assumed spectral index to $\Gamma = 2.5$ changes the presented ULs by less than 2 per cent. Also shown is the HE γ -ray flux from the point-like source 2FGL J1045.0–5941, coincident with Eta Carinae, as detected by the LAT instrument on-board the *Fermi* satellite (Abdo et al. 2009, 2010b; Farnier et al. 2011). Above the energy threshold of 470 GeV , the derived 99 per cent integral flux ULs are $7.7 \times 10^{-13} \text{ ph cm}^{-2} \text{ s}^{-1}$ for a point-like source at the position of Eta Carinae and $4.2 \times 10^{-12} \text{ ph cm}^{-2} \text{ s}^{-1}$ for the extended *Region 2*.

The light curve of the binary system Eta Carinae shows variability in the optical (e.g. Daminieli et al. 2000), IR (e.g. Whitelock et al. 2004), X-ray (Corcoran et al. 2010) and HE γ -ray band (Walter & Farnier 2011) on time-scales of months to years. In order to search for a possible variability in VHE γ rays on similar time-scales, the data collected during the HESS observations between 2004

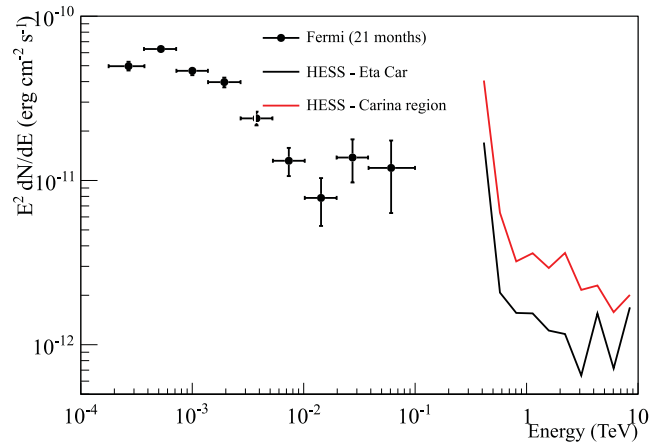


Figure 2. HESS upper limits (99 per cent confidence level) on the VHE γ -ray flux from Eta Carinae and the Carina nebula. Also shown are the spectral points for 2FGL J1045.0–5941 as derived by Farnier et al. (2011). Note that the *Fermi*-LAT spectrum and the HESS ULs have been obtained from data which were not taken contemporarily. Due to the lack of statistics, ULs at higher energies could not be produced.

and 2010 have been split into six different data sets accordingly (see Table 1). Since no VHE γ -ray signal could be found in any of these data sets, flux ULs have been derived for the covered time periods using the same assumptions as before. The statistics, energy thresholds and ULs are summarized in Table 2. Fig. 3 shows the HESS flux ULs (99 per cent confidence level) above 1 TeV at the different orbital phases of Eta Carinae. Also shown are the *RXTE*/*ASM* light curve and the *INTEGRAL*/*IBIS* data points in the X-ray domain as well as the *AGILE* and monthly *Fermi*-LAT light curve in HE γ rays.²

3 DISCUSSION

3.1 Eta Carinae

The detection of point-like HE γ -ray emission from 2FGL J1045.0–5941 was originally reported in the three-month bright source list (Abdo et al. 2009) and was confirmed by Farnier et al. (2011) based on 21 months of data. The spectrum presented by Farnier et al. (2011) shows two distinct features: a low-energy component which is best fitted by a power law with index $\Gamma = 1.69 \pm 0.12$ and exponential cut-off at $1.8 \pm 0.5 \text{ GeV}$ and a HE component which extends to $\sim 100 \text{ GeV}$ and is well described by a simple power law with index 1.85 ± 0.25 . If the HE γ -ray flux shown in Fig. 2 extended to the TeV regime, it would have been detectable in the HESS data presented in this work. The non-detection of a significant VHE γ -ray signal from Eta Carinae at any orbital phase and in the complete HESS data set has some interesting implications for the origin of the HE γ -ray emission which are discussed below.

Walter & Farnier (2011) showed that the flux of the HE component ($E > 10 \text{ GeV}$) decreases by a factor of 2–3 in the yearly light curve, which could point to a scenario in which the parent particle population is accelerated in the colliding wind region of the binary system (Tavani et al. 2009; Bednarek & Pabich 2011; Farnier et al.

² The light curve has been obtained following the procedure described in Farnier et al. (2011), but for an extended data set of 30 months (MJD 54682 to MJD 55595).

Table 2. Statistics and flux upper limits for the HESS Eta Carinae data sets.

Data set	<i>On</i>	<i>Off</i>	α	Excess	Significance (σ)	E_{th} (TeV)	$F_{99}(> E_{\text{th}})$ ($\times 10^{-12}$ photon cm^{-2} s^{-1})	$F_{99}(> 1 \text{ TeV})$ ($\times 10^{-12}$ photon cm^{-2} s^{-1})	Phase
1	70	414	0.1633	2.4	0.3	0.43	2.99	1.29	0.12
2	14	218	0.0543	2.2	0.6	0.43	4.46	1.89	0.29
3	85	2300	0.0383	-3.2	-0.3	0.47	1.78	0.83	0.52
4	29	236	0.0875	8.3	1.6	0.52	2.26	1.17	1.01–1.04
5	350	3744	0.0852	31.1	1.6	0.52	0.64	0.33	1.18–1.21
6	100	2364	0.0426	-0.6	-0.1	0.52	1.23	0.64	1.34–1.35
All	648	11 248	0.0540	40.2	1.6	0.47	0.77	0.36	0.12–1.35

On denotes the number of γ -ray-like events from *Region 1*, *Off* denotes the number of γ -ray-like events from the background control regions, α is the normalization factor between the *On* and *Off* exposures, E_{th} is the energy threshold in TeV, and $F_{99}(> E_{\text{th}})$ and $F_{99}(> 1 \text{ TeV})$ are the 99 per cent flux ULs above E_{th} and 1 TeV, respectively, following Feldman & Cousins (1998).

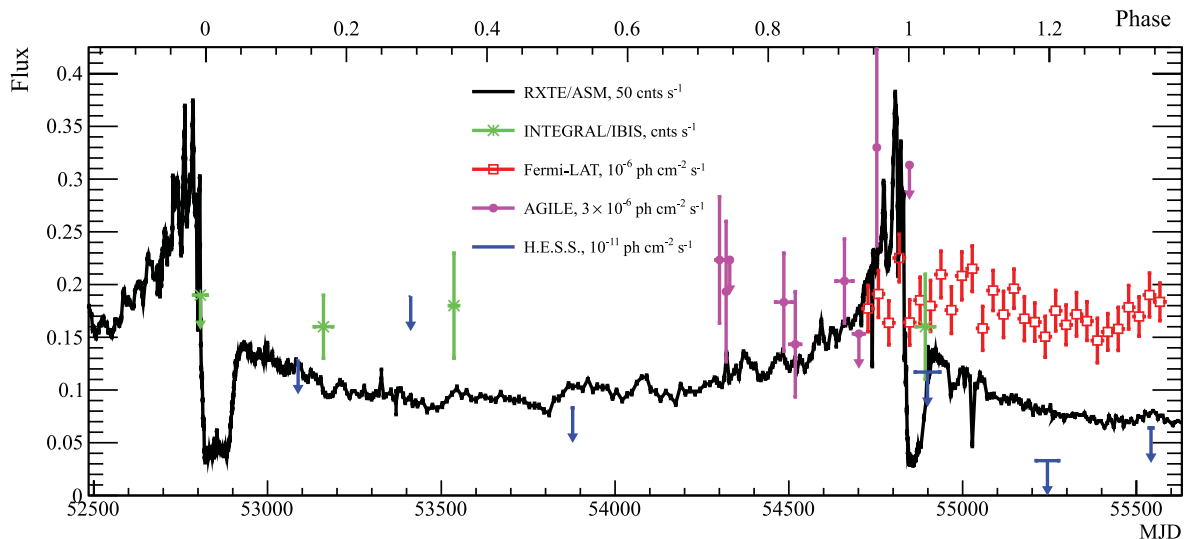


Figure 3. HESS flux upper limits (99 per cent confidence level) for Eta Carinae and the six data sets described in Table 1 (blue). Also shown are the *RXTE/ASM* light curve (black, 50 counts s^{-1} correspond to $\sim 3.75 \times 10^{-10}$ $\text{erg cm}^{-2} \text{s}^{-1}$; Corcoran et al. 2010), *INTEGRAL/IBIS* data points (green, 0.15 counts s^{-1} correspond to $\sim 1.11 \times 10^{-11}$ $\text{erg cm}^{-2} \text{s}^{-1}$; Leyder et al. 2008), *AGILE* measurements (purple; Tavani et al. 2009) and the monthly *Fermi-LAT* light curve (red). The *AGILE* flare is not shown, but it falls around MJD 54753 with a flux of 0.90 ± 0.22 in this representation. Note that the x errors on flux points and ULs indicate the different time periods covered by observations of the different instruments (e.g. Table 1).

2011). However, the low-energy component does not seem to vary on yearly or monthly time-scales. For the colliding wind model, the lower energy component ($0.2 \text{ GeV} \leq E \leq 10 \text{ GeV}$) detected by the LAT is interpreted as inverse Compton (IC) γ -ray emission produced in interactions of the accelerated electrons with the dense stellar radiation fields of the binary stars. The hard HE γ -ray component can be interpreted in the colliding wind region model as either π^0 -decay γ rays, which are produced in proton–proton interactions in the dense stellar wind material (Bednarek & Pabich 2011; Farnier et al. 2011, their Model B) or as a second leptonic IC contribution (Model A in Bednarek & Pabich 2011). Interestingly, the HESS flux ULs for the individual subsets above the threshold energies of $\sim 0.5 \text{ TeV}$ are all well below the extrapolated hard HE γ -ray component measured by *Fermi-LAT* (which is at a level of $\sim 1 \times 10^{-11}$ $\text{erg cm}^{-2} \text{s}^{-1}$).³ This implies that the γ radiation spectrum has a cut-off below $\sim 1 \text{ TeV}$, caused either by a cut-off in the

accelerated particle spectrum or resulting from significant γ - γ absorption in the radiation field close to the two stars in the colliding wind region model. Bednarek & Pabich (2011) concluded that in the case of accelerated protons, the resulting π^0 -decay γ -ray emission should extend to TeV energies at phases far from periastron. The HESS data do not show γ -ray emission in the multi-TeV range at any orbital phase. Note, however, that the maximum detectable photon energy critically depends on the γ - γ absorption at the location where the photon is emitted, and on the alignment between the γ -ray production region, the star and the observer. For Eta Carinae, the optical depth for TeV particles becomes smaller than unity only at phases far from periastron, where the radiation field densities of both stars are low enough to allow γ rays to escape the system (see e.g. fig. 3 in Bednarek & Pabich 2011).

In an alternative scenario, particles are assumed to be accelerated in the outer blast wave which originates in the Great Eruption (Ohm, Hinton & Domainko 2010). For a potential non-variable hadronic HE γ -ray component, as discussed in Skilton et al. (2012), the maximum particle energy of the parent proton population is limited by three different parameters: the time since the giant outburst, i.e. 167 yr, the blast wave speed, which is measured as

³ Note that for a steeper spectral index of the HE LAT component, i.e. $\Gamma \lesssim -2.5$, the HESS ULs of the individual data sets are compatible with the *Fermi-LAT* spectrum.

3500–6000 km s⁻¹ (Smith 2008) and the magnetic field, which is only poorly constrained. Contrary to the effects close to the wind-wind collision region, γ - γ absorption at the location of the blast wave has no significant effect on the γ -ray spectrum, given that the optical depth $\tau_{\gamma\gamma}$ at this location is orders of magnitude smaller than in the colliding wind region. For the parameters used in Ohm et al. (2010),⁴ the maximum energy of protons producing γ rays of 0.5–1.0 TeV energy would be of $\mathcal{O}(5\text{--}10)$ TeV for magnetic field strengths in the blast wave of 3–10 μ G and a blast wave speed of 3500 km s⁻¹. For this set of parameters, the HESS measurement excludes larger magnetic fields and/or higher blast wave speeds for this model.

3.2 Carina nebula

The Carina nebula harbours many potential particle acceleration sites such as massive binary systems (e.g. WR 25, Eta Carinae or the recently discovered HD 93250; Sana et al. 2011), young massive stellar clusters (e.g. Tr 14 and Tr 16) and possibly one or more SNR shells. Electrons and hadrons accelerated at these places would diffuse out of the acceleration region and interact with interstellar radiation fields and/or gaseous material, producing γ -ray emission via π^0 -decay or IC processes. Potential HE or VHE γ -ray emission could therefore trace the regions where a SNR shell interacts with high-density gas in MCs (as observed e.g. for W28; Aharonian et al. 2008b; Abdo et al. 2010). Additionally, low-energy CRs could be traced by ionization of MCs (see e.g. Ceccarelli et al. 2011).

Townsley et al. (2011) investigated the complex structure and composition of the diffuse X-ray emission in the Carina nebula with the *Chandra* satellite. The spectrum of this emission is phenomenologically best described by a multi-component model of different thermal plasmas in collisional ionization equilibrium and in a non-equilibrium ionization state. The X-ray emission does not seem to show any hint of a non-thermal component which would be indicative of particle acceleration in this region. Possible explanations for these observations are e.g. that currently no particle acceleration is taking place and hence non-thermal emission is not expected, or that the potential synchrotron emission has a much lower flux level than the efficient plasma emission, or the SNR shock has been diluted in the ambient plasma. If, however, particle acceleration occurred in the past at e.g. the shocks from one or more potential SNR shells, electrons might have cooled via synchrotron or IC radiation to a level not detectable by *Chandra* or below the HESS UL, respectively. Note that for a far-IR luminosity of $L_{\text{Car}} \sim 7 \times 10^6 L_{\odot}$ (Salatino et al. 2012) and a circular region of 16 pc radius, the IC cooling time for 1 TeV electrons would be $\tau_{\text{IC}} \sim 6 \times 10^3$ yr.

CR hadrons on the other hand diffuse out of the acceleration region and interact with the gaseous or dusty material, producing π^0 -decay γ rays. The HESS ULs can be used to constrain the CR density enhancement factor κ_{CR} in units of the local CR density using equation (10) from Aharonian (1991), assuming that all the gas located in *Region 2* is irradiated by CRs at the same time. Following Preibisch et al. (2011b) and Yonekura et al. (2005), the total gas and dust mass in *Region 2* can be estimated to $\sim 1.5 \times 10^5 M_{\odot}$. At a distance of 2.3 kpc this gives $\kappa_{\text{CR}} = 23/f$, where f is the fraction of the MC mass effectively irradiated by HE CRs. Assuming $f = 1$, this value can be compared to the CR enhancement

factors obtained from the HESS detection of VHE γ -ray emission from W28 (Aharonian et al. 2008b). W28 is an old [(3.5–15) $\times 10^4$ yr; Kaspi et al. 1993], mixed-morphology SNR, which is seen to interact with MCs belonging to the same massive star-forming region (e.g. Brogan et al. 2006). Aharonian et al. (2008b) derive $\kappa_{\text{CR}}(\text{W28}) = 13\text{--}32$ for clouds with masses (0.2–1.5) $\times 10^5 M_{\odot}$ and distances between 2 and 4 kpc. However, there is at present no evidence for a SNR in the Carina nebula, although SN explosions must have already occurred in the past (say $\sim 10^6$ yr ago), in view of the presence of a neutron star. In that case, the lack of GeV–TeV emission from the nebula may have two explanations, separate or combined: (i) the factor f being $\ll 1$ due to diffusive or advective transport of CRs in the region (too slow to fill the region or so fast that they escape), in which case the UL to $k_{\text{CR}} \gg k_{\text{CR}}(\text{W28})$ and/or (ii) the p–p collision time-scale (for an average gas density of 100–400 cm⁻³ in the 50-pc region) is about 10 times less than the age of putative SNRs.

4 SUMMARY

The search for VHE γ -ray emission from the colliding wind binary Eta Carinae and the most active HII region in the Galaxy, the Carina nebula, has been presented. No sign of VHE γ -ray emission could be detected by HESS for Eta Carinae and a 99 per cent UL on the integral γ -ray flux of 7.7×10^{-13} photon cm⁻² s⁻¹ above 470 GeV has been derived using a 33-h data set collected over 6 years and covering the full phase range of the binary. Given the detection of a HE γ -ray component by *Fermi*-LAT, which extends up to ~ 100 GeV, and assuming a spectral index of the HE *Fermi*-LAT component as found for the average spectrum by Farnier et al. (2011), the derived HESS ULs imply a cut-off in the γ -ray spectrum below a few hundred GeV. HESS observations did not reveal significant VHE γ -ray emission from the Carina nebula either. The derived ULs allow us to estimate the CR enhancement factor in this region (< 23) which is at a comparable level to the values obtained for the W28 complex, assuming that CRs illuminate the whole cloud complex. HESS II, which adds a 600 m² telescope to the existing system, will be operational during the next periastron passage in mid-2014 and will be sensitive to lower energies. Together with the future Cherenkov Telescope Array (CTA; Actis et al. 2011), with its greatly improved sensitivity and broader energy coverage, both instruments will close the gap between the HE and VHE γ -ray range and will allow us to probe the cut-off region in the γ -ray spectrum of Eta Carinae and to search for any variability in this system at VHEs.

ACKNOWLEDGMENTS

We thank the referee R. Walter for his helpful comments and suggestions. The support of the Namibian authorities and of the University of Namibia in facilitating the construction and operation of HESS is gratefully acknowledged, as is the support by the German Ministry for Education and Research (BMBF), the Max Planck Society, the German Research Foundation (DFG), the French Ministry for Research, the CNRS-IN2P3 and the Astroparticle Interdisciplinary Programme of the CNRS, the UK Science and Technology Facilities Council (STFC), the IPNP of the Charles University, the Czech Science Foundation, the Polish Ministry of Science and Higher Education, the South African Department of Science and Technology and National Research Foundation, and by the University of Namibia. We appreciate the excellent work of the technical support staff in Berlin, Durham, Hamburg, Heidelberg, Palaiseau, Paris,

⁴ Note that Ohm et al. (2010) work in the limit of Bohm diffusion which might overestimate the particle acceleration efficiency.

Saclay and Namibia in the construction and operation of the equipment. SO acknowledges the support of the Humboldt Foundation by a Feodor-Lynen research fellowship.

REFERENCES

- Abdo A. A. et al. (Fermi-LAT collaboration), 2009, *ApJS*, 183, 46
 Abdo A. A. et al. (Fermi-LAT collaboration), 2010, *ApJ*, 718, 348
 Abdo A. A. et al. (Fermi-LAT collaboration), 2010a, *ApJ*, 723, 649
 Abdo A. A. et al. (Fermi-LAT collaboration), 2010b, Fermi/Large Area Telescope 1 year catalog. http://fermi.gsfc.nasa.gov/ssc/data/access/lat/1yr_catalog/1FGL_catalog_v2.pdf
 Abramowski A. et al. (HESS collaboration), 2012, *A&A*, 537, A114
 Actis M. et al. (CTA consortium), 2011, *Exp. Astron.*, 32, 193
 Aharonian F. et al. (HEGRA collaboration), 2002, *A&A*, 393, L37
 Aharonian F. et al. (HESS collaboration), 2005, *A&A*, 442, 1
 Aharonian F. et al. (HESS collaboration), 2006a, *A&A*, 457, 899
 Aharonian F. et al. (HESS collaboration), 2006b, *ApJ*, 636, 777
 Aharonian F. et al. (HESS collaboration), 2006c, *A&A*, 460, 743
 Aharonian F. et al. (HESS collaboration), 2007a, *A&A*, 467, 1075
 Aharonian F. A. et al. (HESS collaboration), 2007b, *A&A*, 469, L1
 Aharonian F. et al. (HESS collaboration), 2008a, *A&A*, 477, 353
 Aharonian F. et al. (HESS collaboration), 2008b, *A&A*, 481, 401
 Aharonian F. A., 1991, *Ap&SS*, 180, 305
 Albert J. et al. (MAGIC collaboration), 2006, *Sci.*, 312, 1771
 Bednarek W., Pabich J., 2011, *A&A*, 530, A49
 Benbow W., 2005, in Degrange B., Fontaine G., eds, *Proc. Conf. Towards a Network of Atmospheric Cherenkov Detectors VII. Ecole Polytechnique, Palaiseau*, p. 163
 Berge D., Funk S., Hinton J., 2007, *A&A*, 466, 1219
 Bongiorno S. D., Falcone A. D., Stroh M., Holder J., Skilton J. L., Hinton J. A., Gehrels N., Grube J., 2011, *ApJ*, 737, L11
 Brogan C. L., Gelfand J. D., Gaensler B. M., Kassim N. E., Lazio T. J. W., 2006, *ApJ*, 639, L25
 Ceccarelli C., Hily-Blant P., Montmerle T., Dubus G., Gallant Y., Fiascon A., 2011, *ApJ*, 740, L4
 Clark J. S., Larionov V. M., Arkharov A., 2005, *A&A*, 435, 239
 Corcoran M. F., Hamaguchi K., Pittard J. M., Russell C. M. P., Owocki S. P., Parkin E. R., Okazaki A., 2010, *ApJ*, 725, 1528
 Daminieli A., Kaufer A., Wolf B., Stahl O., Lopes D. F., de Araújo F. X., 2000, *ApJ*, 528, L101
 Daminieli A. et al., 2008, *MNRAS*, 384, 1649
 de Naurois M., Rolland L., 2009, *Astropart. Phys.*, 32, 231
 Eichler D., Usov V., 1993, *ApJ*, 402, 271
 Ezoe Y., Hamaguchi K., Gruendl R. A., Chu Y.-H., Petre R., Corcoran M. F., 2008, *PASJ*, 61, S123
 Farnier C., Walter R., Leyder J., 2011, *A&A*, 526, A57
 Feinstein A., 1995, *Rev. Mex. Astron. Astrofis.*, 2, 57
 Feldman G. J., Cousins R. D., 1998, *Phys. Rev. D*, 57, 3873
 Hamaguchi K. et al., 2007, *PASJ*, 59, 151
 Hamaguchi K. et al., 2009, *ApJ*, 695, L4
 Hillier D. J., Davidson K., Ishibashi K., Gull T., 2001, *ApJ*, 553, 837
 Ishibashi K. et al., 2003, *AJ*, 125, 3222
 Kaspi V. M., Lyne A. G., Manchester R. N., Johnston S., D'Amico N., Shemar S. L., 1993, *ApJ*, 409, L57
 Leyder J., Walter R., Rauw G., 2008, *A&A*, 477, L29
 Leyder J., Walter R., Rauw G., 2010, *A&A*, 524, A59
 Li T., Ma Y., 1983, *ApJ*, 272, 317
 Nielsen K. E., Corcoran M. F., Gull T. R., Hillier D. J., Hamaguchi K., Ivarsson S., Lindler D. J., 2007, *ApJ*, 660, 669
 Nolan P. L. et al. (Fermi-LAT collaboration), 2012, *ApJS*, 199, 31
 Ohm S., van Eldik C., Egberts K., 2009, *Astropart. Phys.*, 31, 383
 Ohm S., Hinton J. A., Domainko W., 2010, *ApJ*, 718, L161
 Parkin E. R., Pittard J. M., Corcoran M. F., Hamaguchi K., Stevens I. R., 2009, *MNRAS*, 394, 1758
 Pires A. M., Motch C., Turolla R., Treves A., Popov S. B., 2009, *A&A*, 498, 233
 Pittard J. M., Corcoran M. F., 2002, *A&A*, 383, 636
 Preibisch T. et al., 2011a, *A&A*, 530, A34
 Preibisch T., Schuller F., Ohlendorf H., Pekruhl S., Menten K. M., Zinnecker H., 2011b, *A&A*, 525, A92
 Reimer A., Pohl M., Reimer O., 2006, *ApJ*, 644, 1118
 Salatino M., de Bernardis P., Masi S., Polenta G., 2012, *ApJ*, 748, 1
 Sana H., Le Bouquin J.-B., De Becker M., Berger J.-P., de Koter A., Mérand A., 2011, *ApJ*, 740, L43
 Sekiguchi A., Tsujimoto M., Kitamoto S., Ishida M., Hamaguchi K., Mori H., Tsuboi Y., 2009, *PASJ*, 61, 629
 Skilton J. L., Domainko W., Hinton J. A., Jones D. I., Ohm S., Urquhart J. S., 2012, *A&A*, 539, A101
 Smith N., 2006, *MNRAS*, 367, 763
 Smith N., 2008, *Nat*, 455, 201
 Smith N., Brooks K. J., 2008, in Reipurth B., ed., *The Carina Nebula: A Laboratory for Feedback and Triggered Star Formation*, *Astron. Soc. Pac.*, San Francisco, p. 138
 Smith N., Belly J., Walborn N. R., 2010, *MNRAS*, 405, 1153
 Smith N., Gehr R. D., Hinz P. M., Hoffmann W. F., Hora J. L., Mamajek E. E., Meyer M. R., 2003, *AJ*, 125, 1458
 Tavani M. et al. (AGILE collaboration), 2009, *ApJ*, 698, L142
 Townsley L. K. et al., 2011, *ApJS*, 194, 15
 Walter R., Farnier C., 2011, *Proc. 32nd Int. Cosmic-ray Conf.*, Beijing, <http://galprop.stanford.edu/elibrary/icrc/2011/papers/OG2.2/icrc1076.pdf>
 Whitelock P. A., Feast M. W., Marang F., Breedt E., 2004, *MNRAS*, 352, 447
 Yonekura Y., Asayama S., Kimura K., Ogawa H., Kanai Y., Yamaguchi N., Barnes P. J., Fukui Y., 2005, *ApJ*, 634, 476

This paper has been typeset from a $\text{\TeX}/\text{\LaTeX}$ file prepared by the author.